Generalizing the Abbott-Firestone curve by two new surface descriptors

J. Schmähling, F. A. Hamprecht*

Multidimensional Image Processing,
Interdisciplinary Center for Scientific Computing (IWR),
Im Neuenheimer Feld 368, D-69120 Heidelberg, Germany

Abstract

In surface characterization tasks, the material ratio function is one of the most important tools and the basis for many parameters defined in international standards. Yet, the material ratio does not contain information on spatial features. In this contribution, characterizing functions that generalize the material ratio function approach to include spatial features are presented. These functions can be related to properties such as roughness, fluid flow or connectedness of peaks. In a second step, two classes of surface models for which these characterizing functions can be calculated analytically are presented. By comparing measured and analytically calculated functions, one can estimate model parameters from the characterizing functions, which then serve as simplified surface descriptors. Finally, the capabilities of the introduced methods are illustrated by means of simulations and comparison with experiments.

1   Introduction

In the development and production of an industrial part, both the macroscopic shape and the microstructure of the surface strongly influence its properties. For instance, the microstructure influences the wear behavior of parts in frictional contact or may cause leakage in a gasket. Therefore, the microstructure has to be crafted carefully by using appropriate surface finish tools and the production needs to be supervised in order to ensure the quality of the industrial parts.

1

To get an insight into the surface microstructure, various measurement techniques were developed. The first instruments were tactile profilometers that record the vertical deflection of a stylus that is moved along a line over the surface. As the stylus has permanent contact with the surface, it is easily soiled or damaged.

Furthermore, tactile stylus instruments would usually acquire only a single line profile; the analysis of the microstructure has therefore mostly been limited to two dimensional surface data. More recently, 3D-measuring instruments such as interferometry or fringe projection have become available for surface microstructure inspection. These can acquire an entire 3D height map at once and store it as a 2D image. The optical instruments are fast and contactless and are thus well suited for the application in an industrial environment.

The new 3D measurement devices in combination with fast computers offer new possibilities: It is now possible to study 3D height maps which contain much more information than single profile sections, as the latter could always miss important features of a surface if not recorded in the right position. As 3D height maps are basically 2D images, virtually all methods developed in image processing are also applicable to the analysis of surface microstructure. Techniques include but are not limited to digital filters [6], spectral analysis [13], texture analysis [18] and topographic feature extraction [28].

The availability of an abundance of analysis techniques leads to the so-called "parameter rash" [33], that is the development of too many new, heuristic, and even irrelevant surface microstructure parameters. Successful parameters should allow for a stepwise information/data reduction, capture the characteristics of a surface in a compact way, and have a solid statistical foundation. The Abbott-Firestone curve is a good example, but captures no spatial information at all. In the following sections, a novel analysis technique, which is a direct generalization of the Abbott-Firestone curve is introduced: Section 2 shows how the Abbott-Firestone curve can be extended using techniques from stochastic geometry and how the new characterizing functions can be interpreted; section 3 illustrates how further parameters can be derived from these, and section 4 demonstrates the applicability of the proposed technique.
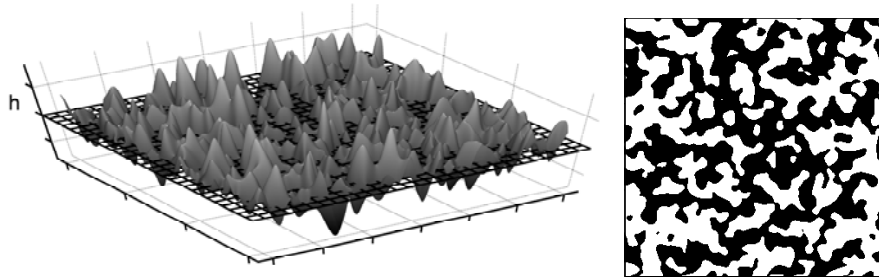
Figure 1: A surface and a level set. The cutting plane is indicated by a mesh in the left image.

2 Stochastic geometry

2.1 The study of level sets

The study of level sets is another image processing technique that has proven its usefulness in many applications. A level set is the result of a thresholding operation, that is, one cuts the surface at a given height and regards the points where the cutting plane hits the material as a set. Its complement is the region where the plane cuts through thin air. Thus, a level set $A_S(h)$ is the set of points in $\mathbb{R}^2$ at which the height of the surface S exceeds the height h (figure 1). Choosing a threshold above the highest surface peak yields an empty set; choosing a threshold below the deepest pit yields the full domain.

The simplest feature of a level set is the relative area, also called the material ratio. This dimensionless value is the ratio between the area of the subset of the sampling window where material is hit by the cutting plane and the whole area of the sampling window. The material ratio ranges from 0 to 1. Calculating the material ratio at different thresholds h yields the material ratio curve (Abbott-Firestone curve, [1]), which is equivalent to the estimated marginal distribution function of a random process. This curve is an important tool in surface characterization, and a large part of the surface characteristics defined in international standards [11] are derived from it (e.g. R_{vk}) or have a direct relation (R_q, R_{sk}, R_{ku}).

Complementary to the material area is the void area, the region where the cutting plane does not hit the material. This void area represents valleys, dales or cavities in the surface. The void area is of interest in tribology as cavities in the surface can serve as lubricant retention pockets. Several
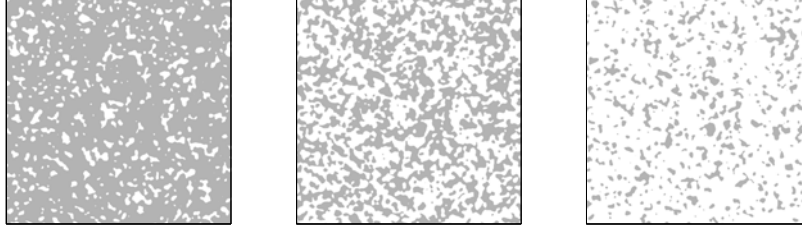
Figure 2: Three 2D-sets with Euler characteristics $\chi = 395, 1, -371$, respectively. White areas represent material, gray represents void areas.

researchers [22, 24] have used the void area in their experiments. In their analysis, two kinds of void areas are distinguished: those which are connected to the border of the workpiece/ measurement window and those isolated from it. The resulting two area functions have been used in a number of tribological applications [5, 23].

Apart from the area, one can also investigate the contour length of the level sets. The contour length obviously contains information on how smooth the level set is. Sets with many or jagged objects will have a greater contour length than sets with a few smooth objects. The contour length of a level set at a fixed height has been used [12] to investigate the surface microstructure of sheet metal.

In addition to contour length and area, the number of isolated void areas (i.e. cavities) or isolated material areas (i.e. peaks) is also of interest. It has been shown [34] that the number of isolated cavities, combined with their contour length and area, can be used to describe the frictional behavior of surfaces. The number of peaks of a surface has also been adopted by international standards [11, 10]. A similar quantity useful for counting objects is the so-called Euler characteristic χ, sometimes also called the genus, which counts the number of objects in a level set minus the number of holes in them (figure 2).

The Euler characteristic has an important interpretation in the context of percolation [16]. A negative Euler characteristic indicates that the material is predominantly characterized by isolated holes. Vice versa, for a positive Euler characteristic, the material would consist mainly of isolated objects. Thus, for a level set with a very low Euler characteristic, a fluid can be expected to be trapped in the holes, while it could flow freely in the case of a high Euler characteristic. Since the Euler characteristic relates to the

possibility of fluid flow on a surface, it may be of great interest in tribological applications [29].

Area, contour length and the Euler characteristic of a 2D set are known in mathematics as Minkowski functionals[1]. In the following section, it will be pointed out in detail how these quantities can be used to describe surfaces.

2.2 Minkowski functionals

The Minkowski functionals, sometimes also called intrinsic volumes or Quermaß integrals, are functionals that describe the shape of sets in $\mathbb{R}^d$ [27][2]. For a set $\mathcal{C} \subset \mathbb{R}^2$, there exist three such functionals, namely the area A, the contour length C and the Euler characteristic χ which is the number of objects minus the number of holes. Surprisingly, the three functionals can be calculated in linear time for discrete binary sets by means of look-up tables [21]. Especially the efficient calculation of the Euler characteristic is remarkable as it does not require complex image segmentation algorithms as one might expect. These three functionals have the following properties in common, as detailed in [15]:

- *Additivity*: For two sets $\mathcal{C}_1$ and $\mathcal{C}_2 \subset \mathbb{R}^2$, $m(\mathcal{C}_1 \cup \mathcal{C}_2) = m(\mathcal{C}_1) + m(\mathcal{C}_2) - m(\mathcal{C}_1 \cap \mathcal{C}_2)$.

- *Motion Invariance*: For any rotation ρ and any displacement t, $m(\rho\mathcal{C}_1 + t) = m(\mathcal{C}_1)$

- *Convex Continuity*: For a convex set $\mathcal{K}$ and a sequence of convex sets $\mathcal{K}_i$ approximating $\mathcal{K}$, also $m(\mathcal{K}_i) \to m(\mathcal{K})$,

where m is one of the functionals A, C or χ.

A famous theorem by Hadwiger [9] states that on the convex ring, every additive, motion invariant and convex continuous measure can be written as a linear combination of the Minkowski functionals. Thus, one can express every level set characteristic that is additive, motion invariant and convex continuous in terms of the Minkowski functionals only; other descriptors will be redundant. This completeness makes the Minkowski functionals a very

---

[1]Strictly speaking, they are proportional to the Minkowski functionals, but the constants will be neglected here.

[2]Thresholding a height map yields a 2D set; hence, only the $d = 2$ case will be considered in the following.
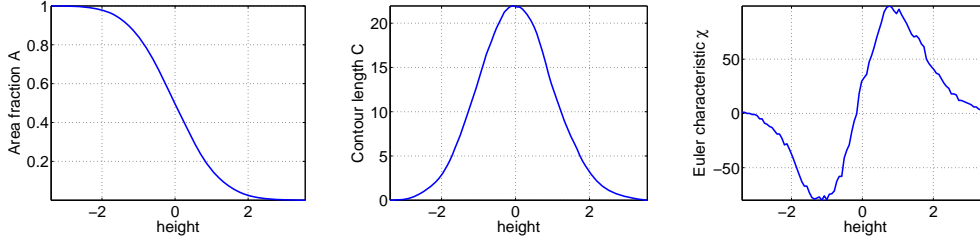
Figure 3: The three characterizing functions for the surface example from figure 1.

important tool for describing sets. Minkowski functionals have been used to solve problems in areas ranging from materials science [20, 4] to astrophysics [14], which strongly encourages an investigation of their usefulness for surface data analysis.

2.3 Characterizing functions and their interpretation

As described in section 2.1, the Minkowski functionals can be calculated for all level sets $A_s(h)$, yielding three functions that can be used to characterize the surface. The area function is, up to normalization, simply the well known Abbott-Firestone curve, and the functions describing contour length and Euler characteristic can be seen as extensions thereof (figure 3)[3].

The Abbott-Firestone curve is often summarized in terms of parameters related to its peak, core and valley part. Similarly, parameters can be derived from the contour length and Euler characteristic function:

- The contour length allows a deeper understanding of a surface's roughness than the Abbott-Firestone curve alone, as the latter does not take spatial information into account. The contour length function can be used to describe spatial features: For surfaces with smooth slopes it will have a lower amplitude than for surfaces with short-wavelength structures. The latter will yield level sets with many small or jagged objects as the surface will cross the threshold very often. Thus, the maximal amplitude can be related to the spatial aspect of roughness (figure 6).

---

[3]For a height map with n pixels, all three functions with k levels can be calculated in $O(kn)$.

6

- For high thresholds, $\chi(h)$ is a good estimate for the number of peaks above this threshold. It is known that for Gaussian random functions, the Euler characteristic of a level set is the number of local maxima plus the number of local minima minus the number of saddle points above this threshold. As there are only a negligible number of minima and saddle points above a high threshold, one can use the Euler characteristic to count peaks. The same result holds for low thresholds, where one can count pits.

- The Euler characteristic can also be used to define a percolation threshold as the height level where the Euler characteristic function has its zero crossing, according to the argument in section 2.1. Usually, there will be only one such height level (figures 5, 7). A high percolation threshold (it is supposed that the surface data has zero mean) suggests better fluid retention properties, as the fluid will not be able to move freely below this threshold.

Overall, these vector-valued parameters express surface properties in a condensed and interpretable form. Plotting the functions for different surfaces under investigation can already reveal a lot about the current task. However, the functions still might contain irrelevant information, and the main information content can often be condensed into few scalar-valued parameters[4]. Second, in practical applications other, more specialized parameters may sometimes be of interest. For surfaces without observable structures, general statistical properties such as the covariance function are sufficient descriptors. On the other hand, for structured surfaces like ground surfaces or surfaces with embedded particles, the structures' properties, e.g. the number and shape of the troughs or particles are of interest.

In the following section, it will be shown how the characterizing functions can be linked to such features. A systematic investigation is most easily performed using surface models, as these can be tailored to one's needs. A finite set of surfaces and the corresponding characterizing functions can be obtained from Monte-Carlo-simulation. But one can do better: For a broad class of surface models, the characterizing functions can be calculated analytically, giving a direct link between model parameters and characterizing functions.

---

[4]This fact is well-known for the Abbott-Firestone curve, which is usually summarized in terms of a few scalar parameters such as the core roughness depth R_k.

3 Models for random surfaces

Once the relation between model parameters and characterizing function is known, the model parameters can be fit such that the deviation between analytically calculated and estimated Minkowski functionals is minimized. The empirical Minkowski functionals can then be interpreted in the context of a specific model. Next, two random models especially suited for technical surfaces are introduced.

3.1 Random fields

The most frequently used and best established model for random surfaces is the random field model [19]. In this model, a random height value is assigned to each point of the reference plane[5] according to a joint distribution. The heights at different points are assumed to depend on each other, thus giving the possibility to model spatial features. In the following, only stationary and isotropic random fields will be considered. Stationary random fields have the same mean in each point, which is assumed to be 0 without loss of generality. That is, the mean over many realizations is 0 in every point. Isotropy means that the relation between two points depends only on their distance but not on the direction of the second point relative to the first. In the following, two important special cases of random fields will be considered:

- Gaussian random fields (GRF) follow a multivariate Gaussian distribution. For a stationary and isotropic GRF, this multivariate distribution can be completely characterized by its covariance function, which depends only on the distance between two points. The use of GRF is often motivated by the central limit theorem of probability theory which states (roughly) that the sum of arbitrary independent random variables tends to a Gaussian distribution. This assumption often applies to practical situations where the machining process consists of many independent events, e.g. in shot-blasting.

- In χ^2 random fields[6], the heights are distributed according to a χ^2 distribution with N degrees of freedom. A χ^2 distribution is the dis-

---

[5]As surface measurements are usually recorded as data on a lattice, the points can be assumed to lie on a grid, corresponding to the pixels of a height map.

[6]The χ in "χ^2 random fields" should not be confused with the Euler characteristic which is also denoted by χ. There is no relation between the two.

8

tribution of the sum of N squared standardized normally distributed random variables. For small N, this distribution is asymmetric; for large N, it tends to a Gaussian distribution. The χ^2 field is of interest because it allows us to model asymmetric distributions. It has been investigated in [3].

- Similar to the χ^2 field, other random fields derived from the Gaussian allow for an analytical investigation. These fields will not be considered here; details can be found in [25, 36].

All the random function models mentioned above are derived from the GRF. Other distributions of practical interest exist, but none of these seem to be theoretically tractable to the extent of the distributions related to the Gaussian. The latter seem to be adequate for the modeling of a wide range of phenomena.

3.2 Boolean models

Random fields model the height distribution in every point of the reference plane; relations between neighboring points are given by a joint distribution. This assumption is not adequate for some surface topographies. For example, consider a ground surface which consists of plateaus separated by troughs. The direction and depth of the troughs will be random, but as one moves along the bottom of a trough, it is clear that the next point will have the same height as the current point. Such a behavior cannot be expressed by random fields, as relations between neighboring points would always be random. The Boolean model, instead, offers the possibility to model randomly located deterministic structures, as observed in the ground surface example.

For instance, some surfaces may be modelled as the union of a set of independently placed, and potentially overlapping, bumps. The projection of the bumps' peaks on an imaginary base substrate yields a pattern of points that are distributed randomly and independently of each other. Each point marks the location of one bump.

The Boolean model is based on such a point pattern, more accurately speaking a Poisson point process [7] in $\mathbb{R}^2$. At each of these random points (also called *germs*), a 3D-object (called a *grain*) of random shape and rotation is placed[7]. Associating to each point in $\mathbb{R}^2$ the maximum of all objects'

---

[7] The original definition of Boolean models uses a point process in $\mathbb{R}^n$ and $\mathbb{R}^n$-grains.

heights in this point yields a 2D-surface embedded in $\mathbb{R}^3$.

In figure 7, two examples of Boolean models are shown. The bottom one is the trough model mentioned earlier, while the top one is a realization of a Boolean model consisting of cylinders of random heights with spherical caps. This model corresponds to the famous Greenwood-Williamson surface model [8]. Greenwood and Williamson model the surface as asperities with a spherical cap having a Gaussian height distribution. Each of these asperities can be seen as a grain of a Boolean model. The grains' height distribution can be chosen to be Gaussian.

3.3 Minkowski functionals of random surface models

For the models presented above, it is possible to calculate the expected Minkowski functionals in terms of the models' parameters. In the following, h will denote the height of the level set.

Gaussian random fields For isotropic stationary zero-mean GRF with certain smoothness constraints, the analytical formulae for the expected Minkowski functionals are [2, 31]

$$
\begin{aligned}
A(h) &= \Phi\left(\tfrac{h}{\sigma}\right) \\
C(h) &= \tfrac{\sqrt{2|\tau|}}{\pi} \exp\left(-\tfrac{h^2}{2\sigma^2}\right) \\
\chi(h) &= \tfrac{h}{\sqrt{2\pi}\sigma} \tfrac{|\tau|}{2\pi} \exp\left(-\tfrac{h^2}{2\sigma^2}\right)
\end{aligned}
\tag{1}
$$

where Φ denotes the cumulative distribution function of the standard normal distribution, σ the standard deviation and τ the second derivative of the covariance function evaluated in 0. Note that the area function depends only on the standard deviation σ, while contour length and Euler characteristic are determined only by σ and the second derivative of the covariance function in 0.

χ^2 **fields** For χ^2 fields with N degrees of freedom, one gets [25]

$$
A(h) = 1 - P\left(\tfrac{h}{2\sigma}, \tfrac{N}{2}\right)
$$

The union of all grains yields a $\mathbb{R}^n$ random set. For a detailed definition of Boolean models and their variants, see e.g. [17].

$$C(h) = \frac{\pi\sqrt{|\tau|}}{2\Gamma(\frac{N}{2})} \left(\frac{h}{2\sigma}\right)^{\frac{N-1}{2}} \exp\left(\frac{-h}{2\sigma}\right) \tag{2}$$

$$\chi(h) = \frac{|\tau|}{2\pi\Gamma(\frac{N}{2})} \left(\frac{h}{2\sigma}\right)^{\frac{N-2}{2}} \exp\left(-\frac{h}{2\sigma}\right) \left(\frac{h}{\sigma} - (N-1)\right),$$

where N is the number of degrees of freedom of the χ^2 distribution, $\Gamma(a) = \int_0^\infty e^{-t} t^{a-1} dt$ the Gamma function, $P(x,a) = \frac{1}{\Gamma(a)} \int_0^x e^{-t} t^{a-1} dt$ the incomplete Gamma function and τ the second derivative of the covariance function evaluated in 0 of the underlying GRF. σ is a scaling factor for the χ^2 distribution similar to the standard deviation of a Gaussion distribution.

Similar expressions for other random fields related to GRF can be derived using the formulae in [25, 36].

Boolean models   For Boolean models [32], the equations

$$A(h) = 1 - \exp\left(-\rho\bar{A}(h)\right)$$
$$C(h) = \frac{2}{\sqrt{\pi}} \exp\left(-\rho\bar{A}(h)\right) \rho\bar{C}(h) \tag{3}$$
$$\chi(h) = \exp\left(-\rho\bar{A}(h)\right) \left(\rho\bar{\chi}(h) - \frac{1}{4\pi}\rho\bar{C}(h)\right)$$

hold, where $\bar{A}(h)$, $\bar{C}(h)$ and $\bar{\chi}(h)$ denote the area, the contour length and the Euler characteristic of the typical grain, i.e. the mean over all grains, and ρ is the density of the underlying point process. If one deals with simply connected grains only, $\bar{\chi}(h)$ is constant 1.

Having equations 1–3 at hand, the influence of a surface's properties on its characterizing functions becomes clear immediately. It is obvious, for example, that in the case of a surface resembling the realization of a GRF, the material ratio depends only on the standard derivation of the underlying Gaussian distribution; both the contour length and Euler characteristic depend on the second derivative of the covariance function evaluated in 0. Thus, contour length and Euler characteristic make it possible to distinguish surfaces with same marginal distribution but different covariance functions.

The Minkowski functionals of Boolean models, instead, depend only on the number of grains and the shape of the typical grain. For example, the Greenwood-Williamson model, which can be regarded as a special case of the Boolean model, assumes grains with a constant cap radius r and a Gaussian grain height distribution. In this case, the formulae for the typical grain become

$$\bar{A}(h) = \int_{u=-\infty}^\infty \pi \, \mathrm{cap}_r(h-u)^2 p_{\mu,\sigma}(u) du = \pi(\mathrm{cap}_r^2 * p_{\mu,\sigma})(h)$$

11
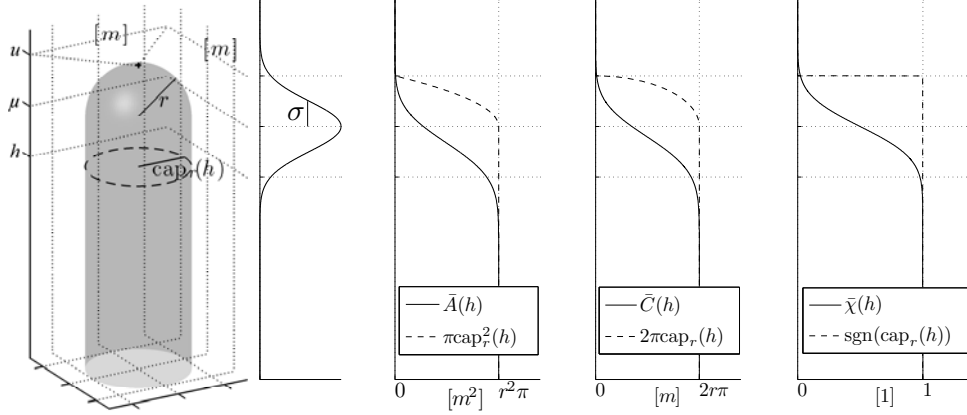
Figure 4: From left to right: A grain with a spherical cap; the Gaussian density describing the probability of the peak height u; the area $\bar{A}(h)$, contour length $\bar{C}(h)$ and Euler characteristic $\bar{\chi}(h)$ of the corresponding typical grain.

$$\bar{C}(h) \quad = \int_{u=-\infty}^{\infty} 2\pi \ \mathrm{cap}_r(h-u)p_{\mu,\sigma}(u)du = 2\pi(\mathrm{cap}_r * p_{\mu,\sigma})(h) \qquad (4)$$
$$\bar{\chi}(h) \quad = \int_{u=-\infty}^{\infty} \mathrm{sgn}(\mathrm{cap}_r(h-u))p_{\mu,\sigma}(u)du = (\mathrm{sgn}(\mathrm{cap}_r) * p_{\mu,\sigma})(h)$$

where $\mathrm{cap}_r(z)$ denotes the radius of the disc resulting from cutting a spherical cap with peak height 0 and radius r at height level z, $p_{\mu,\sigma}$ the normal density function with expectation μ and standard deviation σ, sgn the signum function and $*$ the one-dimensional convolution operator. Together with the number of grains per unit area ρ, eq. 4 can be plugged into eq. 3.

In figure 4, these results are summarized graphically. Note that in contrast to the original grain, the typical grain allows only for a limited geometrical interpretation. In figure 4, for example, $\bar{\chi}$ adopts any value between 0 and 1. The Euler characteristic χ, instead, is an integer for any set.

The convolution in eq. 4 does not allow for a further analytical simplification except in very simple cases, e.g. for grains with a constant height. However, the numerical solution can be found quickly and accurately with standard software packages. Thus, the lack of an analytical solution does not limit the practical use.

3.4 Microcontact models

The above considerations also encourage the use of the Minkowski functionals for the validation or, more accurately, falsification of theoretical results

12

obtained in the domain of surface microcontact models. As stated above, the Minkowski functionals can be calculated for the standard microcontact models. The formulae depend on important model features like the height distribution of peaks, and will thus also reflect changes of the models' parameters. The latter can be used to derive predictions of the surface behavior. If experimental data is available and a model for the surface has been chosen, one can check if the hypothesis based on the model can explain both the estimated Minkowski functionals and the observed surface features, e.g. frictionional behavior. If it turns out that this is not the case, either the assumed model or the hypothesis have to be rejected. This is similar to directly estimating the model parameters from the data and then checking if the surface features are compatible with them, but in practice the Minkowski functionals are usually easier to calculate and more robust estimators.

On the other hand, it is also possible to estimate the models' parameters from the characterizing functions of real data by fitting an appropriate model in terms of the expected characterizing functions. If one assumes the typical grain to be simply connected, thus having a Euler characteristic $\bar{\chi}(h) \equiv 1$, the number of grains and the area and contour length of the typical grain can be uniquely determined from the characterizing functions, which is difficult to achieve by other methods. For Gaussian random fields and χ^2-fields, it would already be sufficient to fit the contour length function: its amplitude is related only to τ, while its extent along the height axis corresponds to the standard deviation of the random function. Nevertheless, it is more informative to fit all three characteristic functions, as this will provide us with more stable results. Furthermore, one can also check how well the empirical functions and the analytically calculated ones match. The selected surface model is tenable only if all three empirical functions match the theoretical well[8].

The authors propose to use the values thus estimated as an amendment to established surface parameters. By using a parametric surface model, a reduced set of characteristics, whose interpretation is straightforward, can be derived. The overall number of parameters which can be defined in this way is limited to the relatively few model parameters, thus limiting the danger of a new "parameter rash".

---

[8]Note that the choice of the model is up to the user. Often, more than model can be used to model the same reality.
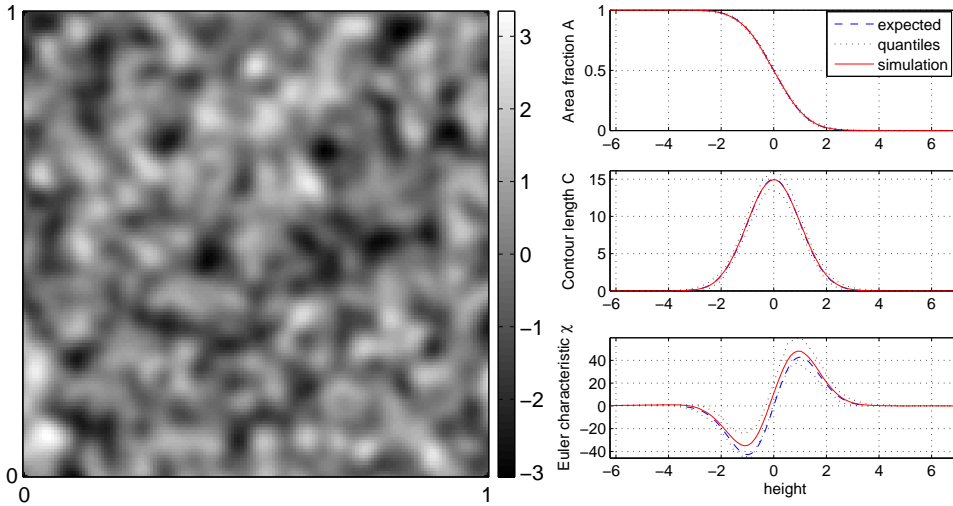
Figure 5: A realization of a Gaussian random field and summarized characteristics for 200 realizations.

4 Experimental results

To show the capabilities of the introduced estimators, various simulations and experiments with real-world data have been performed.

4.1 Simulation results

The first simulation is that of a zero mean stationary Gaussian random field with a Gaussian-shaped, rotation invariant covariance function. The GRF has been simulated by means of the circulant embedding algorithm[35] in a 250×250 pixels window which has by definition area 1. In figure 5, both the measured characterizing functions (solid lines) and their analytically calculated counterparts (dashed line) have been plotted. The dotted lines enclosing the measured characterizing functions show the range which contains 99% of the Minkowski functionals of all 200 realizations.

In spite of the relatively small number of data points, the accuracy of the estimator for area and contour length is remarkable. By choosing a finer grid for the simulation, the measured functions will match the analytically calculated ones even better. For various realizations of the same random process the characterizing functions do not differ significantly, even if the

14

resulting surfaces look different. This underlines the stability of the presented characteristics. Among the three functions, the Euler characteristic shows the largest deviations, followed by the contour length and area ratio. As the Euler characteristic counts every object and every hole, it is the characteristic that is most sensitive with respect to changes in the surface. Unfortunately, the Euler characteristic estimator used in our investigation is biased if calculated for a height map with low resolution. This bias will decrease with higher resolution (see also 4.2).

In figure 6, the results for four other simulations are shown. The characterizing functions were calculated for Gaussian random fields with different covariance function shapes. All four GRF share the same distribution function, i.e. their material ratio function is the same. One observes also that the shapes of the contour length and Euler characteristic functions do not depend on the general shape of the covariance, but only on the value of its second derivative evaluated in 0, τ, as predicted by the analytically calculated functions (eq. 1). The differences in τ show up as different amplitudes of the characterizing function. Since the τ of the second (Gaussian-shaped covariance) and fourth (Bessel type covariance) GRF are the same, also their characterizing functions are almost identical[9]. Nevertheless, the realizations look different especially on longer scales. Accordingly, the characterizing functions cannot provide information on long-wavelength features of the surface. On the other hand, by means of a Taylor series, the covariance functions used can be approximated accurately by a parabola (this information is contained in the characterizing functions via the parameter τ) in the vicinity of 0. Regarding the roughness of a surface, these short-wavelength features are the information one is primarily interested in, as longer wavelengths would be identified with waviness or form and can be separated by a low-pass filter [30].

These results are valid also for the other random fields, and very similar simulation results can be obtained for these.

The second simulation example shows two Boolean models. The grains of the first Boolean model have been chosen to be cylinders of random height with spherical caps and constant diameter (figure 7, upper left). In the second model, the void area is modeled and the grains are troughs with a triangular-

---

[9]In a perfect simulation, the characterizing functions would match exactly if τ was the same. However, as the circulant embedding algorithm [35] used to perform the simulations is only perfect for covariance functions with a finite support, deviations in the characterizing functions occur.
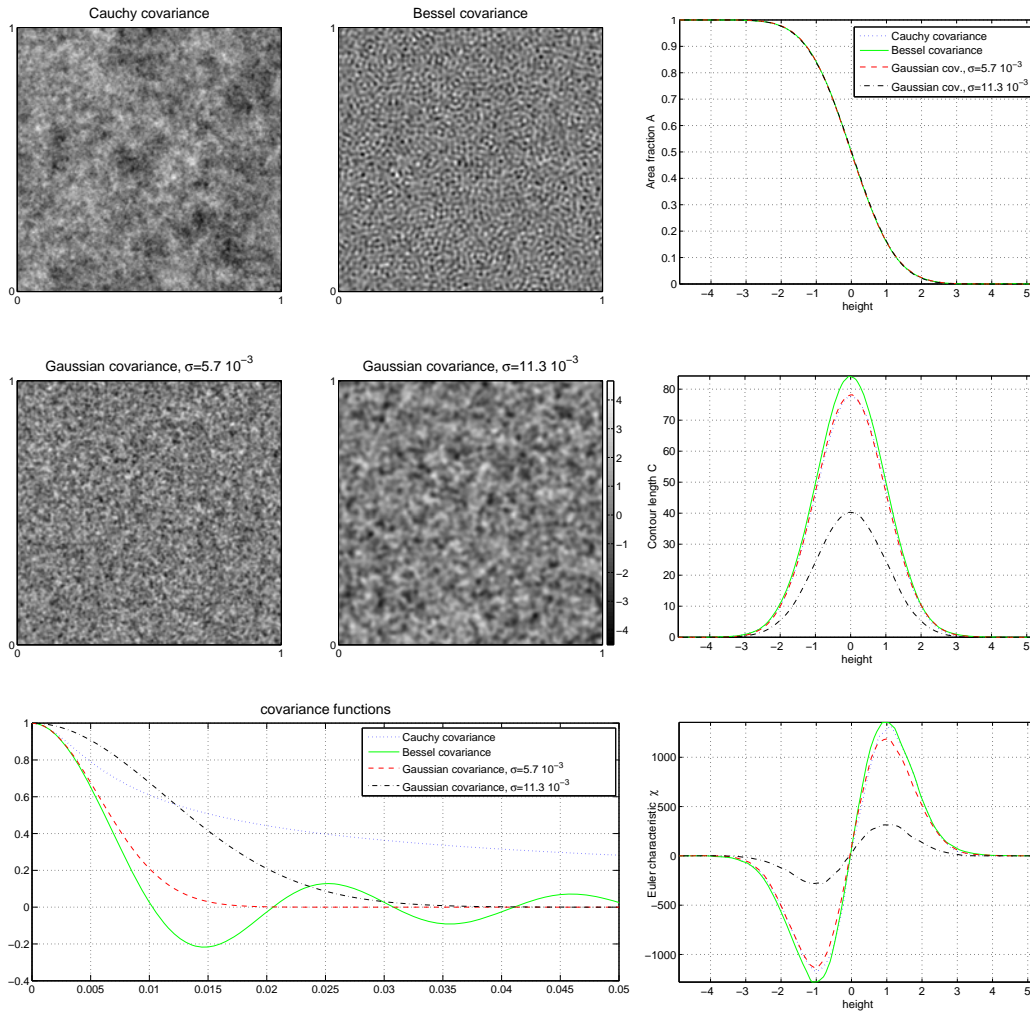
Figure 6: Four realizations of Gaussian Random Fields (GRF) with same standard deviation $\sigma = 1$. All the GRF have the same material ratio function, but different covariance functions. The covariances of the first three GRF have the same parameter τ (the second derivative of the covariance function evaluated in 0).

shaped cross section (figure 7, bottom left). The location and orientation of the troughs is random, but their shape is fixed.

Again, the expected and measured characterizing functions are compared, calculated for 50 realizations with a resolution of 500×500 pixels.

For high thresholds, both estimators are very accurate and analytically calculated and simulated characterizing functions coincide; for low thresholds, the estimators for the trough model become unstable and the calculated contour length and Euler characteristic show a large deviation from their expected values (dashed lines). This can be explained by aliasing effects: In the level sets, sections through the troughs appear as bars, which become narrower as the cutting level is decreased. Finally, the lines become so thin that they cannot be resolved by the chosen pixel resolution. The lines break up in several shorter segments. This causes the formerly connected line-shaped void areas to appear as many small isolated void areas. Thus, the Euler characteristic suddenly falls below zero and shows a large deviation from the expected value. The aliasing effect can be reduced by increasing the sampling rate but will never vanish completely.

4.2   Experiments on shot-blasted surfaces

The shot-blasted surfaces were measured with a NewView Delta white light interferometer (Zygo, Middlefield). The surface (fig. 8) does not show any regular texture. It looks purely random and is therefore likely to match the random field assumption.

Before calculating the characterizing functions, it is necessary to apply a preprocessing filter step. Especially outliers cause high frequencies in the data's Fourier spectrum. As Minkowski functionals tend to concentrate on these high frequencies[10], one would basically describe the noise if applying the characterizing functions to the unfiltered data. A suitable filter to remove outliers is the 3×3 median filter which replaces a height value by the median of the height values in a 3×3 environment. As the filter mask size is small in comparison with the observed extent of the typical microscopic structure, it does not oversmooth and retains the surface structure.

In figure 8, the empirical characterizing functions for the filtered surface are plotted. Analytical expected functions for GRF were fitted using

---

[10]High frequencies are related to the behavior of the autocorrelation function (ACF) close to the origin. The characterizing functions are again related to the ACF behavior at the origin, see section 3.3
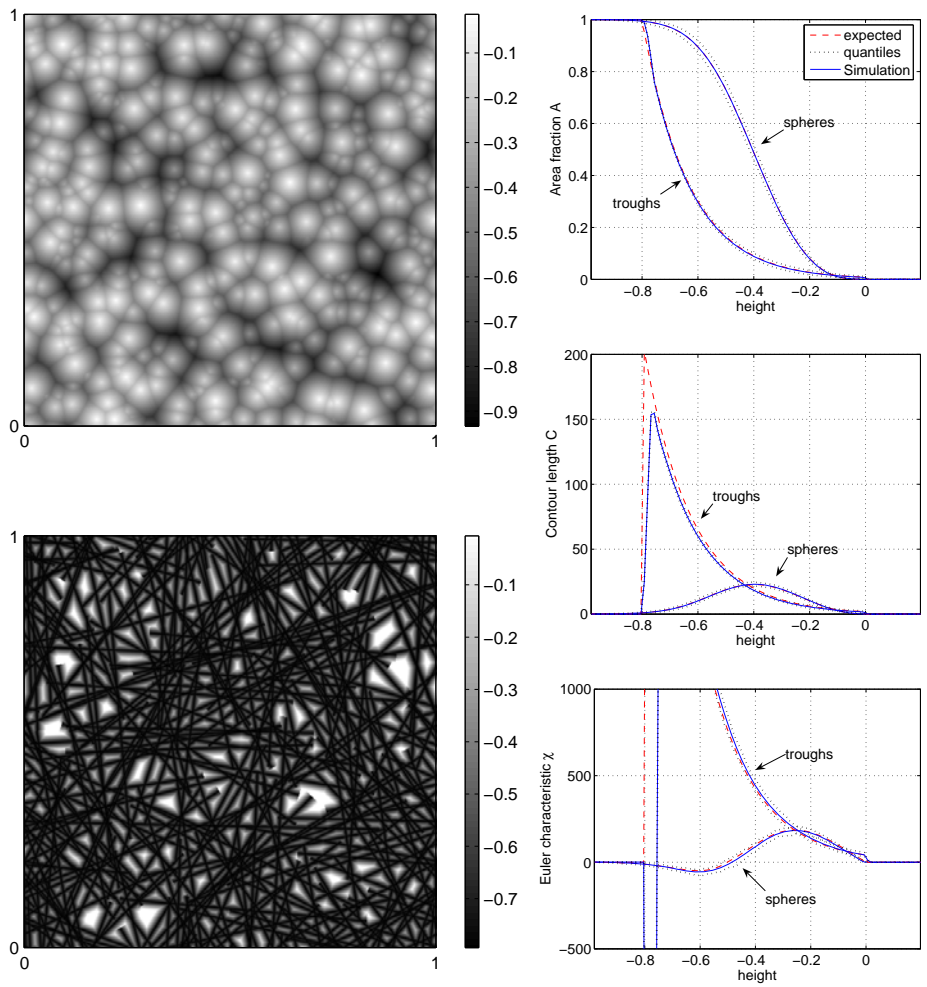
Figure 7: Two realizations of Boolean models and the summarized characteristics of 50 realizations each.
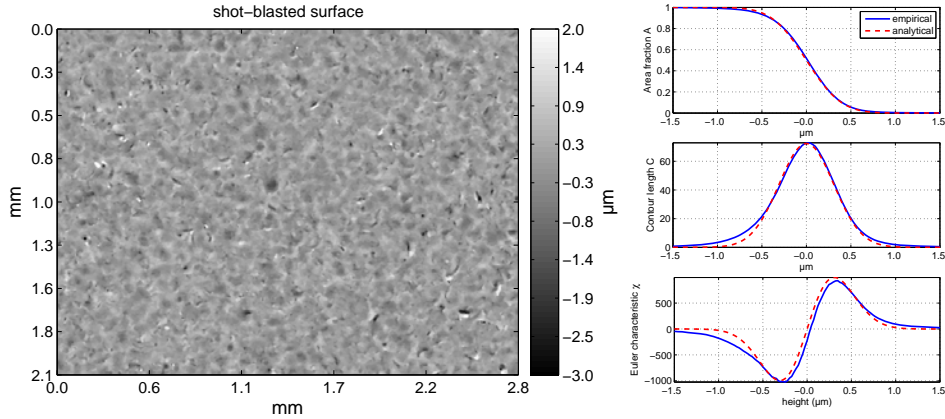
Figure 8: A measurement of a shot-blasted surface and the empirical and fitted analytical characterizing functions.

a weighted least squares minimization according to eq. 1. The deviations between empirical and analytical functions were weighted proportional to the empirical probability density function[11]. Thus, deviations between the functions for high and low thresholds contribute less to the error than deviations in the core part of the surface. The fitted functions show almost perfect coincidence of the fitted and empirical functions in the core part of the surface[12]. Yet the functions' tails cannot be matched exactly; the deviations are higher than those typically observed in simulations (figure 5). It is therefore very unlikely that the data really is a realization of a Gaussian random field. Accordingly, it is not straightforward how the width of the estimated height probability density – this parameter is the most basic parameter to describe surface roughness – should be calculated. The usual approach is to simply estimate the data's standard deviation, which yields the surface roughness parameter R_q or its areal equivalent, S_q. Alternatively, it is possible to fit a Gaussian distribution function to the material ratio function (figure 8). The first approach yields $\sigma = 0.344 \mu m \pm .009 \mu m$[13], the second

---

[11]Weighted least squares methods are common in robust statistics, where one tries to reduce the influence of less reliable data.

[12]The algorithm for estimating the Euler characteristic is still biased; the zero crossing of the Euler characteristic function should coincide with the inflection point of the area characterizing function in theory, but is shifted in practice.

[13]The confidence intervals were estimated by shifting a window of half the height map size over the height map and calculating the Minkowski functionals for each of the windows.

$\sigma = 0.310\mu m \pm .005\mu m$, which is significantly smaller. The reason is that the fit to the characterizing functions focuses on the core part of the surface while the heavier-than-normal tails are almost neglected.

It has to be emphasized that none of the two methods can be regarded as 'superior'; as the surface is not perfectly Gaussian, it is a matter of choice how the Gaussian model is fitted to the data. Nevertheless, the fit using the characterizing functions is more robust as outliers, which will only contribute to high and low levels' Minkowski functionals, will have only a small influence on the estimated parameters.

Similarly to the standard deviation estimation, also the estimation of τ, the autocorrelation's second derivative evaluated in 0, from the shot-blasted surface data yields significantly different results when estimated from the characterizing functions ($\tau = -0.111 \pm .002$) or from the empirical ACF ($\tau = -.100 \pm .002$). A similar effect can be reproduced in simulations if salt-and-pepper noise is added to the simulation. The estimator for $|\tau|$ based on the characterizing functions is more susceptible to noise than the estimate derived from the empirical ACF. This behaviour is plausible: The noise is sparse in relation to the remaining data points and will not have a large impact on the empirical autocorrelation. In contrast, the estimator based on the characterizing function is related to the amplitude of the contour length function which reaches its maximum at threshold $h = 0$. The contour length of the level set at threshold 0 will be considerably larger due to small "holes" and "needles" induced by the noise. The same argument applies to the measurement data, which contains sharp edges. These cause the contour length to become large enough to explain the observed deviation.

As in the following example, the effect described above stresses the importance of a proper preprocessing, which can have significant influence on the results obtained.

4.3 Experiments on sinter material

The sinter material under investigation consists of metal grains which have been fused in a thermal process to form a solid material. A KORAD S18 white light interferometer (3D-Shape, Erlangen) was used to acquire a 1000×1000 height map of the material surface. Neglecting the effect that these grains can only overlap partially in reality, the material structure can be modeled with a Boolean grain model. The grains in the model can be assumed to be cylinders with spherical caps, since a grain appears as a cylinder
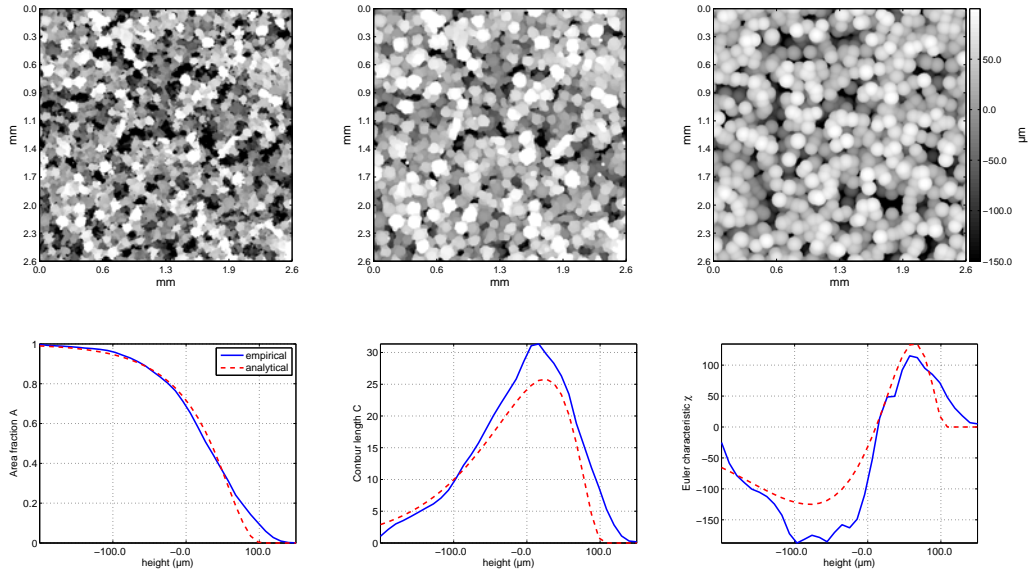
Figure 9: Original, preprocessed and simulated surface of a sinter material and the characterizing functions for the preprocessed and simulated data.

when viewed from above. The cylinders' radius and height are both assumed to be uniformly randomly distributed on a fixed interval.

A measurement of such a surface is depicted in figure 9. A closer look reveals that the single grains are not exactly convex. Since the surface is modeled using cylinders, one has to make the grains more convex. For this purpose, every pixel's height value is replaced by the maximum value of all height values within a circle of radius 6 around the original pixel. This will fill up craters within the grains and smooth recesses in the grains' boundaries. As a consequence, the single grains get slightly larger[14]. In practice, one has to take care not to dilate too much, as the estimators will get unstable if the area fraction approaches 1. Additionally, a 3×3 median filter was applied before the dilation step to remove outliers, since dilating outliers would produce small grain-like artefacts.

Now the characterizing functions can be estimated from the data and the model parameters can be chosen such that the expected characterizing

---

[14]This operation is also known as *gray-value dilation* in the image processing literature. Dilations in the context of random sets lead to so-called contact distributions, an important tool for the analysis of Boolean models. For details, see e.g. [17].
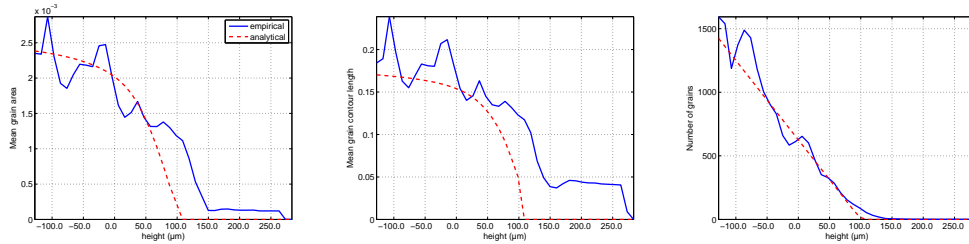
Figure 10: The mean grain characteristics $\bar{A}$, $\bar{C}$ and $\rho\bar{\chi}$ calculated from the estimated characterizing functions

functions (eq. 3) best fit the empirical ones (figure 9)[15]. The fit can be calculated using a least mean square error approach. Although a perfect fit to the empirical characterizing functions is not possible, the model parameters can be chosen in a way to catch the most important features. A simulation with the estimated parameters produces a height map very simular to the real data (figure 9).

Although the simulated surface (figure 9) looks convincing, the deviations between the estimated and the fitted characterizing functions have to be explained. For a better understanding, the equation system 3 is solved for $\bar{A}(h)$, $\bar{C}(h)$ and $\rho\bar{\chi}(h)$. The resulting functions are shown in figure 10. In the transformed functions, the deviations look considerably different. First, one observes that the assumption of uniform distributed heights of the grains is only tenable for the core part of the surface, where $\rho\bar{\chi}(h)$ can be approximated by a straight line. For large thresholds h, where the model assumes no grains, a few grains still exist in practice (see also fig. 9). This also explains that the expected mean grain area and mean grain contour length functions do not follow the estimated functions for large h. Second, the expected grain contour length function lies below the estimated[16]. This is due to the fact that even with the dilation used as preprocessing, the grains in the measurement are still not exactly convex; therefore, the observed mean grain contour length is higher than expected from a convex grain.

These findings show that within the context of a specific model (e.g.

---

[15]The derivation of explicit analytic expressions for $\bar{A}$, $\bar{C}$ and $\bar{\chi}$ in eq. 3 is only practical for very simple models. Instead, numeric integration was used to calculate the expected Minkowski functionals for the model parameters.

[16]The parameters of the model using circular grains cannot be choosen such that both mean grain area and mean grain contour match the estimated values.

Boolean grains), it is possible to compute adjunct descriptors (e.g. $\bar{A}$, $\bar{C}$ and $\bar{\chi}$) that capture the entire information content, and are more directly interpretable in terms of that model (e.g. as describing grain shape).

5   Conclusions

A novel method for the evaluation of 3D surface data has been presented. It is based on stochastic geometry and generalizes the well-known Abbott-Firestone curve, which has been widely accepted in metrology, by associating to it two easily interpretable functions. While the interpretation of the Abbott curve alone does not provide spatial information, the three characterizing functions based on the Minkowski functionals can be related to features like spatial roughness or percolation.

One limitation of the method is that it cannot characterize long-range spatial features. In the Gaussian random field examples (section 4.1), it has been shown that two surface's Minkowski functionals can be the same even if their long-wavelength characteristics differ. However, the surface microstructure is usually investigated in the high-frequency range. Low frequency/long-wavelength features can be separated by waviness and form filters and treated separately. Vice versa, noise that would significantly change the estimated covariance function shape around zero, and therefore also the characterizing functions, can be removed by adequate digital filters.

The advantage of the three obtained characterizing functions is that they can be applied to completely different surfaces. The Minkowski functionals offer the possibility to analyze different models in a unified context. Using Minkowski functionals, it is possible to analyze analytically both random field models (e.g. the Nayak model) and Boolean models (e.g. the Greenwood-Williamson model) using the same characteristics. These two model classes cover both surfaces without observable structures as well as surfaces with repeated structural elements.

Especially the analysis of 3D Boolean models in the presented form is, to our knowledge, new and has not been used in rough surface characterization before. Boolean models are suited for modeling asperities of rough surfaces or surfaces consisting of smaller particles. Using the Minkowski functionals, the mean shape as well as the mean peak curvature of these objects can be estimated easily.

Finally, within the context of specific models, it is possible to derive

adjunct descriptors that may be easier to interpret, thus offering further possibilities to derive simple parameters for surface description.

References

[1] E. J. ABBOTT AND F. A. FIRESTONE, *Specifying surface quality: a method based on accurate measurement and comparison*, Mechanical Engineering, 55 (1933), pp. 569–572.

[2] R. J. ADLER, *The Geometry of Random Fields*, John Wiley & Sons, 1981. Wiley Series in Probability and Mathematical Statistics.

[3] R. J. ADLER AND D. FIRMAN, *A non-Gaussian model for random surfaces*, Physical Transactions of the Royal Society of London. Series A, Mathematical and Physical Sciences, 303 (1981), pp. 433–462.

[4] J. BECKER, G. GRÜN, R. SEEMANN, H. MANTZ, K. JACOBS, K. R. MECKE, AND R. BLOSSEY, *Complex dewetting scenarios captured by thin-film models*, Nature Materials, 2 (2003).

[5] F. BENATI, F. SACERDOTTI, B. J. GRIFFITHS, C. BUTLER, J. M. KARILA, M. VERMEULEN, H. HOLTKAMP, AND S. GATTI, *Correlation between surface topography and lubricant migration in steel sheets for the autobody manufacturing process*, Measurement Science and Technology, 13 (2002), pp. 785–791.

[6] S. BRINKMANN, H. BODSCHWINNA, AND H.-W. LEMKE, *Accessing roughness in three dimensions using Gaussian regression filtering*, International Journal of Machine Tools and Manufacture, 41 (2001), pp. 2153–2161.

[7] W. FELLER, *An introduction to probability theory and its applications. - Vol. 1*, Wiley, 1968. Feller.

[8] J. A. GREENWOOD AND J. B. P. WILLIAMSON, *Contact of nominally flat surfaces*, Proceedings of the Royal Society London, Series A, 295 (1966), pp. 300–319.

[9] H. HADWIGER, *Vorlesungen über Inhalt, Oberfläche und Isoperimetrie*, Springer, 1957.

[10] ISO TC 213 Workgroup 16, *Geometrical Product Specifications (GPS) - Surface Texture: Areal - Part 2: Terms, Definitions and Surface Texture Parameters*, 2005. Standard proposal N756.

[11] *ISO 4287:1997. Geometrical Product Specifications (GPS) – Surface Texture: Profile method*, 1997.

[12] K.-H. Kopplin, *Kennwerte zur Charakterisierung von Feinblechoberflächen.* Private communication, 2003.

[13] J. McCool, *Characterization of surface anisotropy*, Wear, 49 (1978), pp. 19–31.

[14] K. R. Mecke, T. Buchert, and H. Wagner, *Robust morphological measures for large-scale structure in the universe*, Astronomy and Astrophysics, 288 (1994), pp. 697–704.

[15] K. R. Mecke and D. Stoyan, eds., *Statistical Physics and Spatial Statistics*, vol. 554 of Lecture Notes in physics, Springer, Berlin, 2000, ch. Statistical Analysis of Large-Scale Structure in the Universe, pp. 36–71.

[16] K. R. Mecke and H. Wagner, *Euler characteristic and related measures for random geometric sets*, journal of Statistical Physics, 64 (1991), pp. 843 – 850.

[17] I. S. Molchanov, *Statistics of the Boolean model: From the estimation of means to the estimation of distributions*, Advances in Applied Probability, 27 (1995), pp. 63–86.

[18] N. Myshkin., A. Grigoriev, S. Chizhik, K. Choi, and M. Petrokovets, *Surface roughness and texture analysis in microscale*, Wear, 254 (2003), pp. 1001–1009.

[19] P. R. Nayak, *Random process model of rough surfaces in plastic contact*, Wear, 26 (1973), pp. 305–333.

[20] J. Ohser and F. Mücklich, *Statistical Analysis of Microstructures in Materials Science*, John Wiley & Sons Ltd., New York, 2000.

[21] J. Ohser, B. Steinbach, and C. Lang, *Efficient texture analysis of binary images*, Journal of Microscopy, 192 (1998), pp. 20–28.

[22] M. Pfestorf, U. Engel, and M.Geiger, *3D-surface parameters and their application on deterministic textured metal sheets*, International Journal of Machine Tools and Manufacture, 38 (1998), pp. 607–614.

[23] U. Popp, T. Neudecker, U. Engel, and M. Geiger, *Surface characterization with regard to the tribological behaviour of sheet metal in forming process*, in Proceedings of the SheMet '99, M. Geiger, H. Kals, B. Shirvani, and U. P. Singh, eds., 1999.

[24] F. Sacerdotti, F. Benati, C. Butler, and B. Griffiths, *Closed regions: a proposal for spacing parameters for areal surface measurements*, Measurement Science and Technology, 13 (2002), pp. 556–564.

[25] J. Schmalzing, *On Statistics and Dynamics of Cosmic Structure*, PhD thesis, Ludwig-Maximilians-Universität München, 1999.

[26] J. Schmähling, *Statistical characterization of Technical Surface Microstructure*, PhD thesis, Faculty of Mathematics and Computer Science, Ruprecht-Karls-Universität Heidelberg, Heidelberg, 2006. http://www.ub.uni-heidelberg.de/archiv/6792.

[27] M. Schmitt, *Mathematical morphology for shape description*, Journal de Physique IV, 12 (2002), pp. 87–116.

[28] P. J. Scott, *Pattern analysis and metrology: The extraction of stable features from observable measurements*, Proceedings of the Royal Society London, Series A, 460 (2004), pp. 2845–2864.

[29] J. Staeves, *Beurteilung der Topografie von Blechen im Hinblick auf die Reibung bei der Umformung*, PhD thesis, TU Darmstadt, 1998.

[30] M. L. Stein, *Interpolation of Spatial Data - Some Theory for Kriging*, Springer, 1999.

[31] H. Tomita, *Statistics and geometry of random interface systems*, in Formation, Dynamics and Statistics of Patterns, K. Kawasaki, M. Suzuki, and A. Onuki, eds., vol. 1, World Scientific, 1990, pp. 113–156.

26

[32] W. WEIL, *The estimation of mean shape and mean particle number in overlapping particle systems in the plane*, Advances in Applied Probability, 27 (1995), pp. 102–119.

[33] D. J. WHITEHOUSE, *Parameter rash: is there a cure?*, Wear, 83 (1982), pp. 75–78.

[34] A. WIHLBORG AND L. GUNNARSSON, *A frictional study of uncoated EBT steel sheets in a bending under tension friction test*, Wear, 237 (2000), pp. 129–136.

[35] A. WOOD AND G. CHAN, *Simulation of stationary gaussian processes in $[0,1]^d$*, Journal of Computational and Graphical Statistics, 3 (1994), pp. 409–432.

[36] K. WORSLEY, *Local maxima and the expected Euler characteristic of excursion sets of χ^2, F and t-fields*, Advances in Applied Probability, 13 (1994).